Materials Today Bio 32 (2025) 101695

Contents lists available at ScienceDirect

Materials Today Bio

journal homepage: www.journals.elsevier.com/materials-today-bio

LNP-encapsulated miRNA29b for corneal repair: A novel approach to combat fibrosis

Dongyan Li [a], Jing Ji [a,*], Xinyue Li [a], Yi Xie [a], Yan Huang [a], Junzhi Qin [a], Xili Ding [b,**], Lizhen Wang [a,c], Yubo Fan [a,b,***]

[a] Key Laboratory of Biomechanics and Mechanobiology, Ministry of Education, Beijing Advanced Innovation Center for Biomedical Engineering, School of Biological Science and Medical Engineering, Beihang University, Beijing, 100191, China
[b] School of Engineering Medicine, Beihang University, Beijing, Beijing, 100191, China
[c] Innovation Center for Medical Engineering & Engineering Medicine, Hangzhou International Innovation Institute, Beihang University, Hangzhou, 311115, China

ARTICLE INFO

Keywords:
Corneal fibrosis
MicroRNA29
Lipid nanoparticles
Corneal epithelial wound healing

ABSTRACT

Severe corneal injuries often result in corneal scarring, leading to visual impairment and corneal blindness. Currently, there is a lack of effective anti-corneal fibrosis drugs in clinical practice. MicroRNA-based therapies hold significant potential in combating fibrosis. However, the barrier function of the cornea and the fluid environment of the ocular surface reduce drug permeability and bioavailability, presenting significant challenges for local drug application. This study employs microfluidic technology to encapsulate miRNA29b in lipid nanoparticles (LNP) to create an LNP-miRNA29b delivery system (LNP-mir29b) for treating corneal mechanical injuries. *In vitro* experiments show that LNP-mir29b significantly inhibits the expression of α-smooth muscle actin (α-SMA) in an induced corneal stromal cell fibrosis model. *In vivo* experiments using rabbit corneal mechanical injury models indicate that LNP-mir29b effectively reduces fibrosis in the corneal stroma, promotes organized rearrangement of stromal collagen fibers, and decreases the expression of fibrosis-related genes, including Col1A2, Col3A1, Fn, and α-SMA. Additionally, LNP-mir29b accelerates the migration of corneal epithelial cells, promotes wound healing of the epithelium, restores the structural integrity of the corneal epithelium. The LNP system proposed in this study offers a novel approach with anti-fibrotic functionality, providing a new strategy for reducing scarring during the corneal injury repair process.

1. Introduction

Severe corneal injuries, such as those caused by infections, trauma, inflammation, or degeneration, can lead to the development of corneal scars, which reduce transparency and cause visual impairment, ultimately resulting in corneal blindness—a significant global health issue affecting over 10 million people worldwide [1,2]. The organized arrangement of collagen fibers in the corneal stroma is crucial for corneal transparency [3]. The specialized corneal stromal cells (also called keratocytes) within the stroma play a key role in maintaining transparency by synthesizing and secreting collagen and proteoglycans [4]. In response to injury, corneal stromal cells can transform into myofibroblasts, leading to the disorganized deposition of extracellular matrix components and the formation of fibrotic scars, which cause corneal opacity [5]. Currently, there is a lack of effective drugs for treating corneal scarring in clinical practice, and once corneal scarring progresses to a severe stage, the only viable treatment option is corneal transplantation [6,7]. However, the significant shortage of donor tissue and the high cost of the procedure result in prolonged waiting periods for most patients [8]. Therefore, there is an urgent need to develop effective strategies to inhibit scar formation during corneal injury recovery, to restore corneal transparency and visual function.

MicroRNA (miRNA) is a class of small non-coding RNAs with 21–23 nucleotides in length and regulates gene expression at the translational and transcriptional levels [9,10]. Due to the advantages of target specificity, multifunctionality, and potential for non-invasive delivery, miRNA has been widely used in the treatment of a variety of diseases in recent years. Previous studies have demonstrated that the miRNA29

* Corresponding author.
** Corresponding author.
*** Corresponding author. School of Engineering Medicine, Beihang University, Beijing, Beijing, 100191, China.
E-mail addresses: jingji09714@buaa.edu.cn (J. Ji), xiliding@buaa.edu.cn (X. Ding), yubofan@buaa.edu.cn (Y. Fan).

https://doi.org/10.1016/j.mtbio.2025.101695
Received 6 November 2024; Received in revised form 11 March 2025; Accepted 20 March 2025
Available online 22 March 2025

family represses collagen expression and the development of fibroplasia in the regulation of a variety of organ fibrosis [11], including myocardial fibrosis [12], hepatic fibrosis [13], pulmonary fibrosis [14] and cutaneous fibrosis [15]. Moreover, research suggests that human corneal stromal stem cells with high expression of miRNA29a in extracellular vesicles exhibit improved corneal anti-scarring effects in cell-based therapy [16]. This suggests that miRNA29 family may be a crucial therapeutic agent for inhibiting fibrosis during corneal injury repair. Nevertheless, in therapeutic applications, miRNAs typically require a delivery system to protect and enhance *in vivo* efficiency [17]. However, the unique environment of the cornea presents a challenge in delivering miRNA29 family to the site of injury.

The corneal topical administration, due to its safety, convenience, and non-invasive nature, is the most common route for corneal drug apply [18]. However, factors such as nasolacrimal drainage, ocular metabolism, and the blood-ocular barrier can cause a rapid decline in drug concentration before reaching the target tissue [19]. Lipid nanoparticles (LNP) are an effective drug delivery system for enhancing drug permeability, offering good biocompatibility, and have been validated in ocular tissues [20]. Additionally, LNP can better protect nucleic acid drugs due to their bilayer phospholipid structure, which provides stable encapsulation and shields the nucleic acids from degradation [21]. Many LNP-based miRNA delivery systems have already been applied in disease treatment, with some having progressed to the clinical trial stage [22–24]. However, there are no reports documenting the use of LNP as carriers for miRNA-based drugs aimed at reducing corneal scarring.

In response to these challenges, this study developed an LNP-miRNA29b delivery system (LNP-mir29b) for anti-scarring therapy following corneal injury. Using microfluidic technology, miRNA29b was efficiently encapsulated into LNP. Then the LNP-mir29b were applied to an induced corneal stromal cell fibrosis model and rabbit corneal mechanical injury models. The results demonstrated that LNP-mir29b exhibited strong anti-scarring effects both *in vitro* and *in vivo*, significantly reducing the expression of fibrosis-related genes. Furthermore, LNP-mir29b accelerated corneal epithelial wound healing, contributing to the overall restoration of corneal thickness and structure.

2. Materials and methods

2.1. Preparation of LNP formulations

The miRNA29b agomir with the following sequence: sense 5′-UUC UCC GAA CGUGUC ACG UTT-3′, antisense 5′-ACG UGA CAC GUU CGG AGAATT-3′) was synthesized by Suzhou GenePharma Co., Ltd.

LNP containing miRNA29b or without miRNA29b were formulated using microfluidics as previously described [25,26]. The miRNA was dissolved in 33.3 mM sodium acetate solution (pH 4.0). Ionizable cationic lipid 1,2-dilinoleyloxy-3-dimethylaminopropane (DLin-MC3-DMA), 1,2-distearoyl-sn-glycero-3-phosphocholine (DSPC), cholesterol, and 1,2-dimyristoyl-rac-glycero-3-methoxypolyethylene glycol-2000 (DMG-PEG2000) (50:10:38.5:1.5 mol ratios), were dissolved in anhydrous ethanol to a total lipid concentration of 50 mM. Using two syringe pumps, the miRNA-water phase solution and the lipid-ethanol phase solution were mixed in a 3:1 ratio at flow rates of 3 mL/h and 1 mL/h, respectively, through a Y-shaped microfluidic chip. The ratio of miRNA to total lipid was 0.05 in the wild type (WT/WT). The resulting solution was collected using enzyme-free sterile water. The obtained solution was dialyzed using 10K MWCO Slide-A-Lyzer dialysis cassettes (Thermo Fisher Scientific) in Phosphate-buffered saline (PBS) (Gibco).

2.2. Characterization of LNP-mir29b and LNP

To prepare LNP for transmission electron microscope (TEM), LNP were dialyzed against water and stained with 3 % uranyl acetate for negative staining. Imaging was then conducted using a transmission electron microscope (H-7650, Hitachi, Japan).

Samples were dispersed in deionized water (mass fraction of 0.1 %) and ultrasonicated for 3 min. Characterize the average particle size and distribution/Zeta potential of LNP-mir29b using Zetasizer Nano-ZS90 (Malvern Instruments). Particle size and surface charge were measured at 25 °C by using a standard operating procedure.

2.3. Encapsulation efficiency of miRNA

To calculate the miRNA encapsulation efficiency, Quanti-iT RiboGreen RNA reagent assay (Thermo Fisher Scientific) was used as previously described [25]. The working solution was then further diluted 1:1 in TE buffer and TE buffer with 4 % Triton-X100. Unencapsulated miRNA and total miRNA (including miRNA encapsulated in LNP and free miRNA) were measured separately. Each sample was supplemented with 100 μL of a 2000-fold diluted Quanti-iT™ RiboGreen RNA reagent in a 96-well plate, and the fluorescence intensity was detected using a plate reader at an excitation wavelength of 480 nm and an emission wavelength of 520 nm. The EE was calculated as follows: EE (%) = (1 - free miRNA concentration/total miRNA concentration) x100.

2.4. Uptake of the LNP-mir29b

FITC-labeled LNP-mir29b was prepared by replacing 1 mol% DMG-PEG2000 with 1,2-distearoyl-sn-glycero-3-phosphoethanolamine-N-[(polyethylene glycol)-2000]-Fluorescein (DSPE - PEG2000 -FITC) and using the similar microfluidic method. The FITC-labeled LNP-mir29b was topically instilled into the eye (50 nM, 20 μL per hour per eye). After 24 h, the rabbits were euthanized, and their whole corneas were immediately excised. A confocal laser-scanning microscope was used to image the central 6-mm diameter corneal region.

2.5. Cell culture

For human corneal epithelial cells (HCE-T) (Bohui Biological Technology Co., Ltd), cells were cultured in Dulbecco's Modified Eagle Medium/Nutrient Mixture F-12 medium (DMEM/F12) (Gibco) supplemented with 10 % fetal bovine serum (FBS) (Gibco), 1 % (v/v) penicillin-streptomycin (Gibco), 10 ng/mL human epidermal growth factor (hEGF) (Sigma) and 5 μg/mL insulin (Sigma).

Primary rabbit corneal stromal cells (RCSC) were extracted from fresh New Zealand rabbit cornea. After the clearing of the corneal epithelium and endothelium by gentle scraping and rinses, the central stroma (8 mm diameter) was isolated and trimmed into small pieces for digestion with 1 mg/mL Type II collagenase (Sigma). Cells were cultured in DMEM/F12 with 10 % FBS, 1 % (v/v) penicillin-streptomycin (Gibco). Cells from early passages ($\leq$2) were used in all experiments.

Primary rabbit corneal stromal fibroblasts (RCSF) were derived from RCSC via induction with 0.5 ng/mL of transforming growth factor β1 (TGF-β1) (Novoprotein) for 48 h. Following incubation, the induced results were validated through changes in cellular morphology and the expression of the fibroblast marker α-smooth muscle actin (α-SMA).

2.6. Live-dead staining assay

The HCE-T, RCSC, and RCSF were seeded into 12-well plates at a density of 1 × 10^5 cells per well and incubated with different concentrations of LNP-mir29b (0, 12.5, 25, 50, 100 nM) for 48 h. Then, the cells were stained with a live/dead double dye kit (AbMole) according to the manufacturer's instructions. The cells were observed and the images were collected using an Olympus IX73 digital camera.

2.7. Assessment of cell proliferation

The HCE-T, RCSC, and RCSF were seeded into 24-well plates at a density of 7 × 10^3 cells per well. After adding different concentrations of LNP-mir29b (0, 12.5, 25, 50, 100 nM), cell proliferation was

evaluated every 12 h with the Cell Counting Kit-8 (CCK-8) (Beyotime) according to the manufacturer's instructions. Absorbance values at 450 nm were obtained with a microplate reader (Thermo Fisher Scientific).

2.8. Migration assay

The HCE-T, RCSC, and RCSF were seeded and grown to complete confluency in a 6-well plate and scratch wound assays were performed. Briefly, a scratch was created across the center of the monolayer using a sterile pipette tip. Wounded cells monolayers were washed three times with PBS to remove loose cells and debris, and incubated with different concentrations of LNP-mir29b (0, 12.5, 25, 50, 100 nM) for the designated periods, respectively. Photographs of the wounded area were taken under a phase contrast microscope and analyzed by ImageJ software to evaluate the migration among different groups.

2.9. Immunofluorescent staining

For phenotype identification, cells growing on slides were washed three times with PBS and fixed with 4 % (w/v) paraformaldehyde for 30 min. Then, cell permeabilization was performed with 0.2 % (v/v) Triton X-100 (Sigma) for 7 min, and the cells were blocked with 5 % (v/v) fetal bovine serum (Gibco) for 20 min, followed by incubation with primary antibodies (α-SMA, Sigma, 1:200) at 4 °C overnight. The next day, the cells were incubated with secondary antibodies for 2 h. Hoechst dye (Gibco) was used to stain the nuclei. The cells were examined under a confocal laser-scanning microscope (Andor Dragonfly 500, Leica), and images were analyzed by ImageJ software.

2.10. Rabbit corneal injury model

All adult female New Zealand white rabbits (2.0 kg) were housed and treated according to the ARVO statement for the Use of Animals in Ophthalmic and Vision Research with ethics approval from the Ethics Committee of Beihang University (approval number: BM20230219). General anesthesia was induced via intramuscular injection of 3 % sodium pentobarbital at a dose of 3 mL/kg, combined with topical anesthesia achieved using proparacaine hydrochloride eye drops. Briefly, the cornea was marked with a 6 mm trephine, and a surgical knife was used to remove the corneal epithelium and part of the stromal layer, with a depth of approximately 100 μm [27]. Then, liposomes solution (20 μL) without miRNA29b (LNP group, n = 5), with miRNA29b (LNP-mir29b group, n = 5) was administered to the wound area in the left and right eyes, respectively, twice a day.

2.11. Quantitative PCR analysis

Total RNA was extracted by TRIzol (Invitrogen), according to the supplier's directions. The quality of RNA samples was determined according to A260/A280 (values between 1.8 and 2.1). The reverse transcription of RNA was accomplished by using a 1st Strand cDNA Synthesis Kit (Yeasen) and performed qPCR analysis with Hieff qPCR SYBR Green Master Mix (Yeasen). The mRNA expression results were calculated by the$2^{-\Delta\Delta Ct}$ method., and the expression of GAPDH was used as the control. Specific primers for qPCR are listed in Table 1.

Table 1
Specific primers for qPCR.

Gene	Forward Primer (5′-3′)	Reverse Primer (5'>3′)
COL1A2	CAGTGGCGTCGTGCCT	CTGAGCAGCAAAGTTCCCG
COL3A1	CCTAAGGGAGATCCAGGCCC	CGCCAATTCCTCCTATGCCA
FN	ACCCTTATAGCTGTGAAAGGCA	GGGTCGTACACCCAACTTAAA
α-SMA	AACCCTGTTGACTGAGGCAC	AGTCCAGCACAATGCCAGTT
GAPDH	CAGTGCTAGCGCGTCCC	TGCCGTGGGTGGAATCATAC

2.12. In vivo therapeutic evaluation

At the predetermined times, corneal fluorescence staining and slit-lamp examinations were performed to assess the wound healing outcomes. At the same time, cross-sectional images of cornea were obtained by anterior segment optical coherence tomography (AS-OCT) (VG200D, Intalight) to evaluate the cornea repairment. On day 14 post-operation, rabbits were sacrificed, and their corneas were enucleated for histological analysis. The corneal tissues were fixed with 4 % (w/v) paraformaldehyde overnight, embedded in paraffin, and sliced into 5-μm thick sections. The sections were then stained with HE, Masson's trichrome, PAS, and EVG stains according to the manufacturer's instructions (Beyotime). For immunostaining, tissue sections underwent antigen retrieval, blocking, and incubation with primary antibodies (CK3, Santa Cruz, 1:200; ZO-1, Thermo Fisher Scientific, 1:200; α-SMA. 1:200). The next day, the sections were incubated with secondary antibodies, and the nuclei were stained with Hoechst. Histological images were captured by Panoramic MIDI automatic digital slide scanner and confocal laser-scanning microscope, and analyzed using ImageJ software.

2.13. Transmittance measurement

The absorbance of the central 6-mm-diameter corneal buttons was measured over a wavelength range of 280–800 nm, with a step size of 20 nm, using a UV–Vis spectrophotometer (Evolution Pro, Thermo Fisher Scientific). Briefly, immediately after the rabbits were euthanized, the corneas were excised from the sclera. A 6.0-mm central button was obtained from each cornea using a trephine. Each corneal button was placed into a stainless-steel sheet insert with a matching 6-mm hole, sandwiched between two quartz glass plates, and then positioned inside a standard quartz cuvette. For each spectrophotometric measurement, an insert with a thickness matching the corneal sample was used [28]. The obtained data were processed to calculate the transmittance of samples [29].

2.14. Statistical analysis

All data were performed using Prism 8 (GraphPad). Data were expressed as mean ± standard deviation (SD). Student's t-test was used for two-sample statistical comparison, while one-way analysis of variance (ANOVA) followed by Tukey's test was used for groups greater than two. For all experiments, * was used for $p < 0.05$, ** for $p < 0.01$. Specific comparisons are indicated in the respective figure legends.

3. Results

3.1. Synthesis and characterization of the LNP-mir29b

LNP was employed as a drug delivery system to validate the therapeutic potential of miRNA29b in treating corneal injury and preventing fibrosis. LNP-mir29b and LNP formulations, with and without miRNA29b, were prepared (Fig. 1A). Transmission electron microscopy revealed no significant morphological differences between the two formulations (Fig. 1B). For the morphological characteristics of LNP and LNP-mir29b, both platforms generated nanoparticles with a single intensity and number distribution peak, indicating a single particle population (Fig. 1C). LNP-mir29b tended to agglomerate into larger particles (409.5 nm), whereas LNP remained uniform particles (142.6 nm) (Fig. 1C). Zeta-potential data indicated that the addition of miRNA29b agomir changed the charge (Fig. 1D). In addition, the LNP-mir29b formulations demonstrated an encapsulation efficiency of over 85 %.

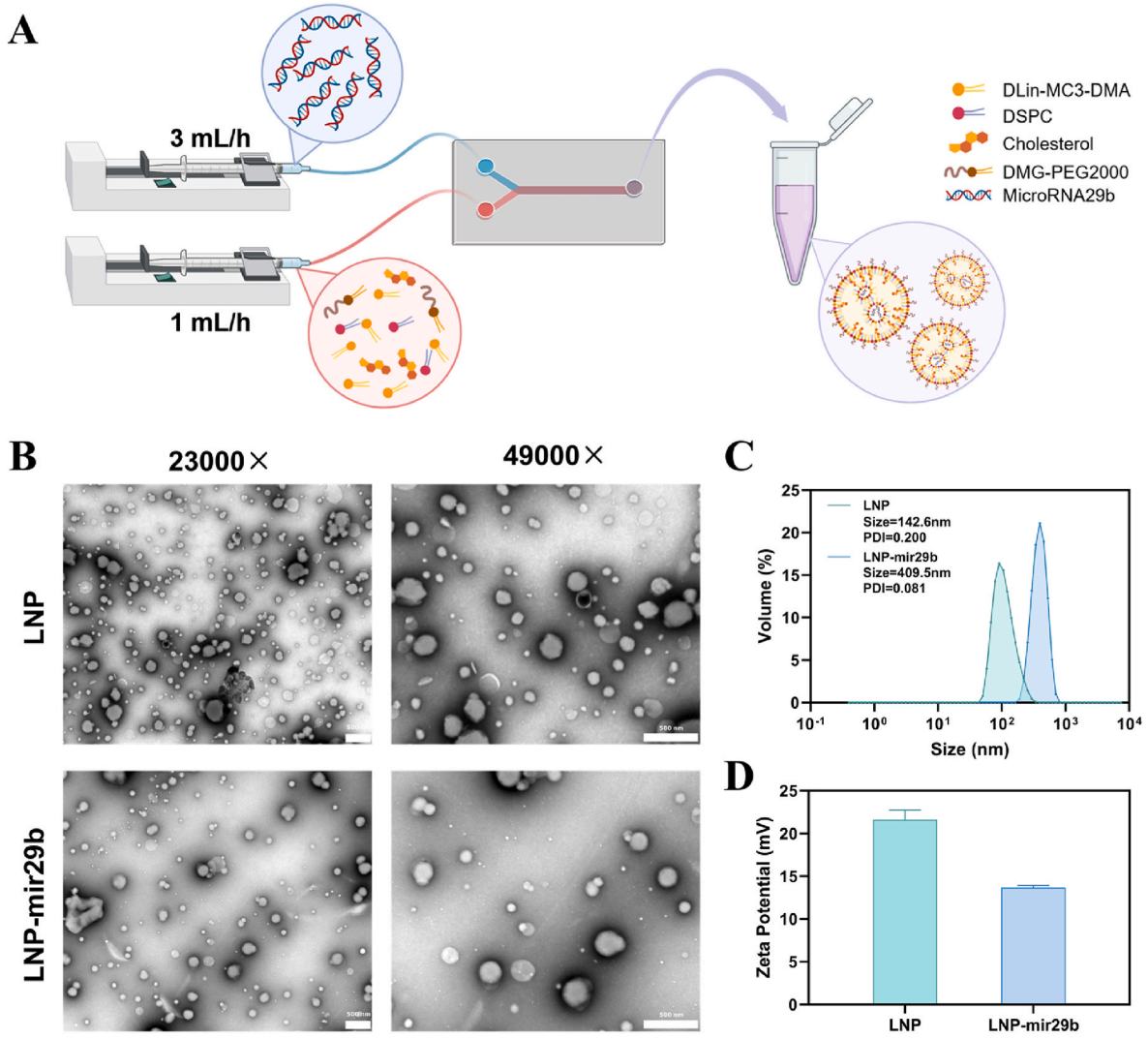

Fig. 1. Characterization of LNP and LNP-mir29b. A) Schematic representation of the preparation process for LNP-mir29b formulations. B) TEM images of LNP-mir29b and LNP. Scale bars: 500 μm. C) The average particle sizes of LNP-mir29b and LNP. D) The zeta potentials of LNP-mir29b and LNP. $n = 3$.

3.2. *In vitro cytocompatibility*

The biocompatibility of LNP-mir29b was validated by incubating immortalized HCE-T, RCSC, and RCSF with different concentrations of LNP-mir29b for 48 h. As shown in Fig. 2A–D, cell viability was not affected at concentrations ranging from 12.5 to 100 nM, as indicated by live/dead staining. Further CCK-8 assays demonstrated that while LNP-mir29b stimulation did not affect the proliferation of HCE-T and RCSC, it significantly inhibited the proliferation of RCSF (Fig. 2E–G). Overall, these results suggest that LNP-mir29b exhibits excellent biocompatibility, evidenced by the viability and proliferation of cells.

3.3. *LNP-mir29b promoted epithelial wound healing and inhibited corneal stromal cell fibrosis in vitro*

To investigate the effect of LNP-mir29b on the migration, different concentrations of LNP-mir29b were applied to assess wound healing rates. Wound healing was assessed at the 24-h incubation time point. The results showed that LNP-mir29b significantly increased cell migration ability and accelerated the wound healing of HCE-T (Fig. 3A and B), whereas the effects on RCSC and RCSF were not statistically significant (Fig. 3C and D; Fig. S1, Supporting Information). Additionally, TGF-β1 was used to induce a stable transformation of RCEC into an RCSF phenotype, followed by treatment with LNP-mir29b, LNP, or miRNA29b alone (Fig. S2; Fig. S3 Supporting Information). The results indicated that LNP-mir29b incubation effectively reduced the expression of α-SMA in TGF-β1-induced corneal fibroblasts in a dose-dependent manner (Fig. 3E and F; Fig. S3 Supporting Information).

3.4. *LNP-mir29b promoted epithelial healing and improved corneal transparency in vivo*

The *in vivo* LNP-mir29b tracking experiment showed that numerous FITC-labeled LNP-mir29b were detected within the wound gaps on the ocular surface, with clear infiltration into the deeper corneal layers (Fig. S4, Supporting Information). During the 14-day treatment period, bright-field observations and AS-OCT images consistently showed that the corneas in the LNP-mir29b group maintained higher transparency. In contrast, starting from day 3, the central injury area of the corneas in the LNP group became noticeably opaque, with progressive worsening over time, showing no signs of resolution even on day 14 post-operation (Fig. 4A–C). The isolated corneal tissues from the LNP group exhibited substantial corneal scarring (Fig. 4D). Quantification of corneal tissue transparency using a UV–Vis spectrophotometer revealed that the LNP-mir29b group had significantly higher transmittance than the LNP group (Fig. 4G). Fluorescein sodium staining and AS-OCT imaging

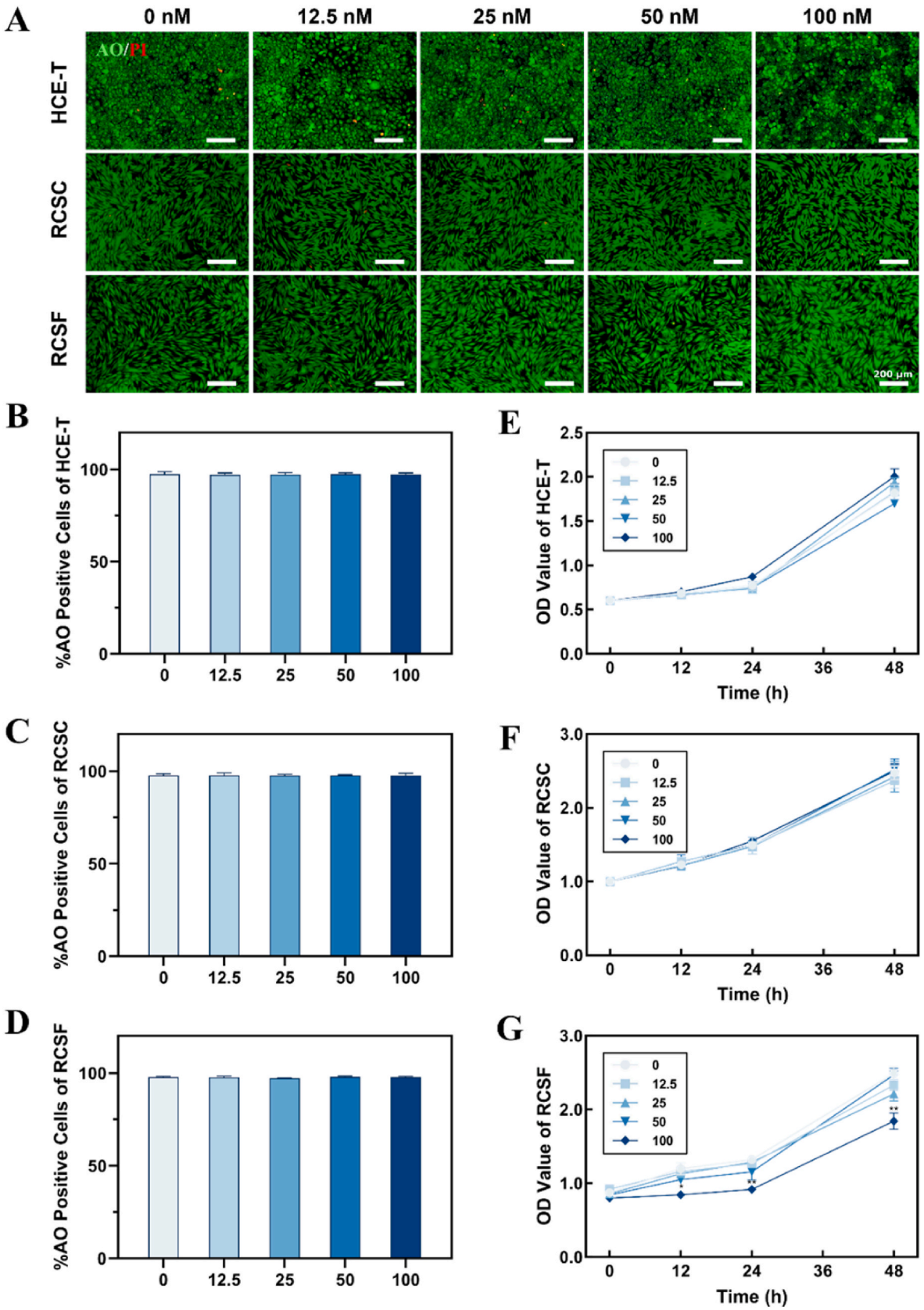

Fig. 2. *In vitro* cytocompatibility of LNP-mir29b. A) Live/Dead staining results of HCE-T, RCSC, and RCSF under the treatment with different concentrations (0, 12.5, 25, 50, and 100 nM) of LNP-mir29b for 48 h. Live cells appeared green in color (acridine orange stain) and dead cells appeared red (propidium iodide stain). Scale bars: 200 μm, $n = 3$. Statistical analysis of AO-stained positive cells of B) HCE-T, C) RCSC, and D) RCSF under the treatment with different concentrations of LNP-mir29b for 48 h $n = 3$. CCK-8 assay of E) HCE-T, F) RCSC, and G) RCSF under the treatment with different concentrations of LNP-mir29b for 0, 12, 24, and 48 h $n = 3$, $^{*}p < 0.05$, $^{**}p < 0.01$.

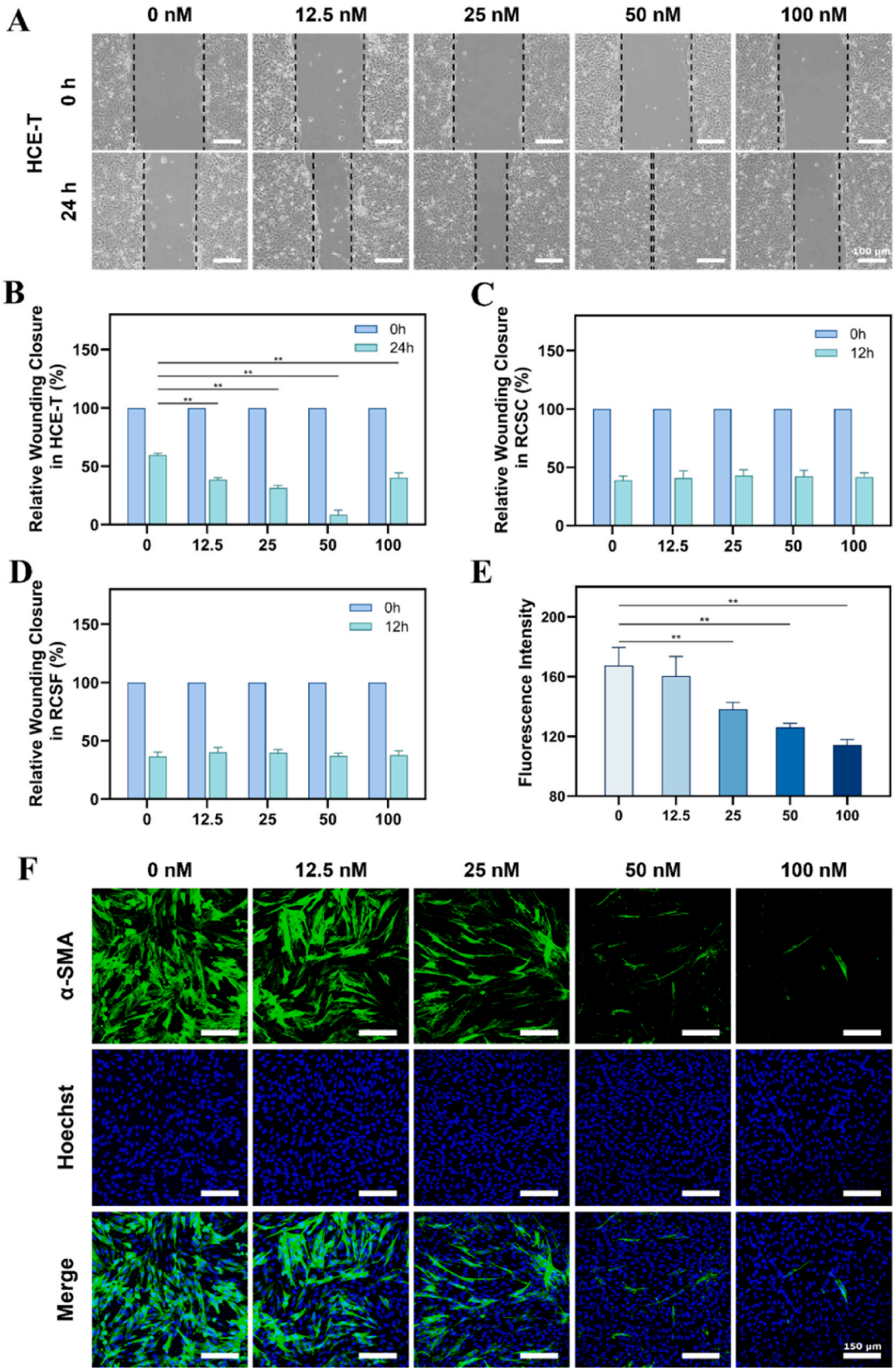

Fig. 3. LNP-mir29b promoted epithelial wound healing and inhibited corneal stromal cell fibrosis *in vitro*. A) Images of scratch wound assay on HCE-T treated with different concentrations (0, 12.5, 25, 50, and 100 nM) of LNP-mir29b. Scale bars: 100 μm. $n = 3$. Statistical analysis of relative wounding closure rates in B) HCE-T, C) RCSC, and D) RCSF treated with different concentrations of LNP-mir29b at 24h. $n = 3$. E, F) Representative immunofluorescent images with statistical analyses of α-SMA staining of RCSF treated with different concentrations LNP-mir29b for 48h. Scale bars: 150 μm. $n = 5$, $^{**}p < 0.01$.

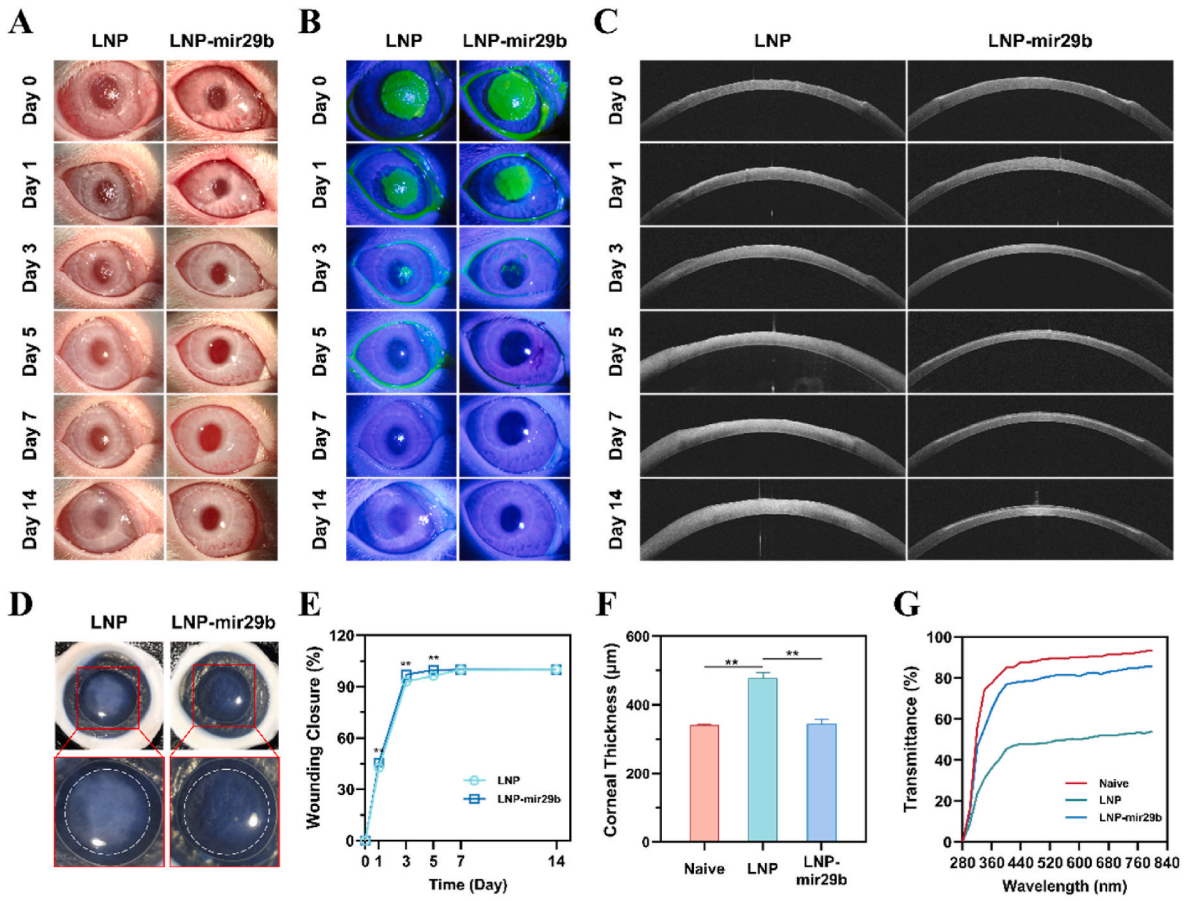

Fig. 4. LNP-mir29b promotes epithelial healing and improves corneal transparency following anterior stromal injury in rabbits *in vivo*. A, B, C) Representative brightfield images, Fluorescein sodium staining images and AS-OCT images of rabbit corneas treated with LNP and LNP-mir29b at different time points (day 0, 1, 3, 5, 7, and 14 post-operation). $n = 5$. D) Representative isolated corneal tissue images treated with LNP and LNP-mir29 at day 14 post-operation. E) Quantification of epithelial wounding closure rate at different time points. $n = 5$. F) Quantification of corneal thickness according to the AS-OCT results at day 14 post-operation. $n = 5$, $^{**}p < 0.01$. G) Changes in transmittance of Naïve, LNP, and LNP-mir29b at day 14 post-operation. $n = 5$.

demonstrated that by day 3 post-operation, re-epithelialization was completed in the LNP-mir29b group, whereas residual corneal defects persisted in the LNP group until day 5 (Fig. 4B, C, E). To further quantify corneal recovery, AS-OCT images were used to measure central corneal thickness in the defect area on day 14 (Fig. 4F). The corneal thickness in the LNP-mir29b group (345.47 ± 12.77 μm) showed no significant difference from that of the naïve group (340.69 ± 2.97 μm). In contrast, the LNP group exhibited corneal edema, with a thickness of 478.72 ± 15.92 μm, which was significantly greater than that of the LNP-mir29b and naïve groups. Consistently, hematoxylin and eosin (HE) staining of corneal tissue sections also revealed substantial corneal thickening in the LNP group (Fig. 5A–E). Throughout the 14-day observation period, no subjects exhibited signs of inflammation, glaucoma, or other complications. In summary, LNP-mir29b reduced stromal scarring, promoted stromal injury recovery, and accelerated corneal epithelial wound healing.

3.5. LNP-mir29b mediated corneal antifibrotic and tissue repair effects by inhibiting fibrosis-related gene expression and promoting epithelial regeneration

Rabbit corneal tissues isolated from the LNP group and LNP-mir29b group after 14 days of treatment, along with naive corneas, were sectioned. HE staining showed that the corneal structure in the LNP-mir29b group closely resembled that of the naïve group, whereas in the LNP group, the corneal epithelium exhibited indistinct boundaries with the corneal stroma and significant infiltration of inflammatory cells (Fig. 5A). Masson's trichrome staining revealed that the corneal epithelial layer appeared red, and the stromal collagen fibers were uniformly stained blue. The LNP group showed increased red staining in the anterior stromal region, indicating an increase in muscle fibers compared to the LNP-mir29b and naive groups (Fig. 5B). Elastica van Gieson (EVG) staining demonstrated that both the LNP-mir29b and naive groups exhibited a dark purple-black corneal epithelium and a reddish-purple stromal layer. In contrast, the LNP group showed intensified dark purple-black staining in the anterior stromal layer, indicative of elastic fiber deposition (Fig. 5C). Periodic Acid-Schiff (PAS) staining showed that the corneal epithelium appeared light purple and the stroma appeared light pink in LNP-mir29b and naive group. However, the LNP group exhibited significantly enhanced deep pink-purple staining in the anterior stromal layer, indicative of increased fibrin deposition (Fig. 5D). To further quantify corneal epithelial repair, HE-stained images were analyzed. The corneal epithelial layer thickness in the LNP group (19.89 ± 4.79 μm) was significantly thinner compared to both LNP-mir29b group (33.39 ± 6.64 μm) and naïve group (34.33 ± 1.45 μm) (Fig. 5F).

Immunofluorescence staining of tissue sections revealed the presence of the terminal differentiation marker Cytokeratin 3 (CK3) in the regenerated corneal epithelium (Fig. 6A). The regenerated corneal epithelium in LNP-mir29b group was composed of 5–7 layers, with a thickness of 34.59 ± 3.40 μm, closely resembling that of the naive group (34.40 ± 2.21 μm). In contrast, the LNP group displayed a significantly thinner corneal epithelium, with a thickness of 19.92 ± 4.97 μm, compared to both LNP-mir29b and naive groups, and the epithelial layer

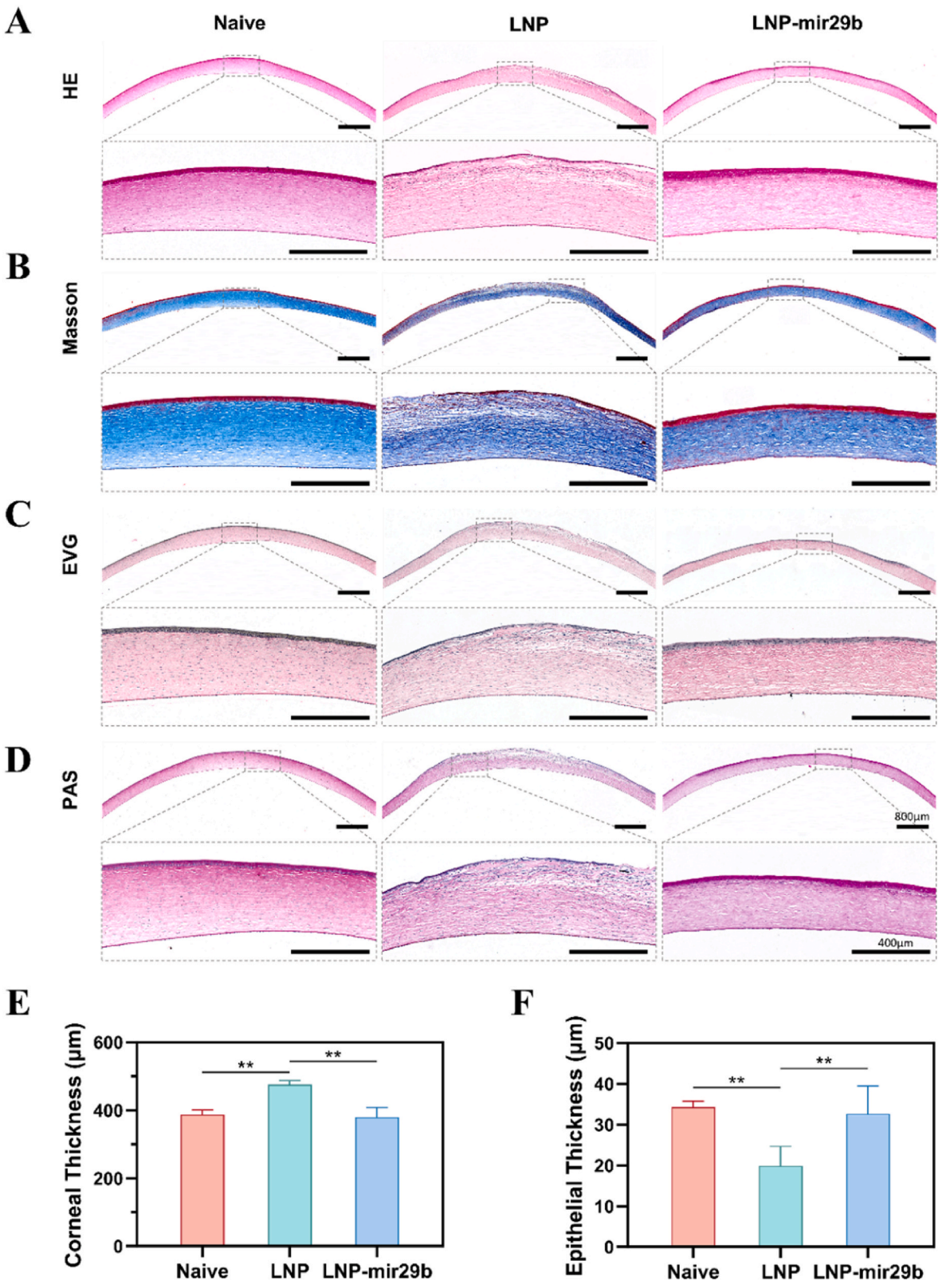

Fig. 5. LNP-mir29b promotes corneal structural recovery post-operation in rabbits *in vivo*. Representative images of A) HE, B) Masson, C) EVG and D) PAS staining on day 14 post-operation of Naïve, LNP, and LNP-mir29b groups. Scale bars: 800 and 400 μm. $n = 5$. Quantification of E) corneal thickness and F) corneal epithelial thickness according to the HE staining results. $n = 5$, $^{**}p < 0.01$.

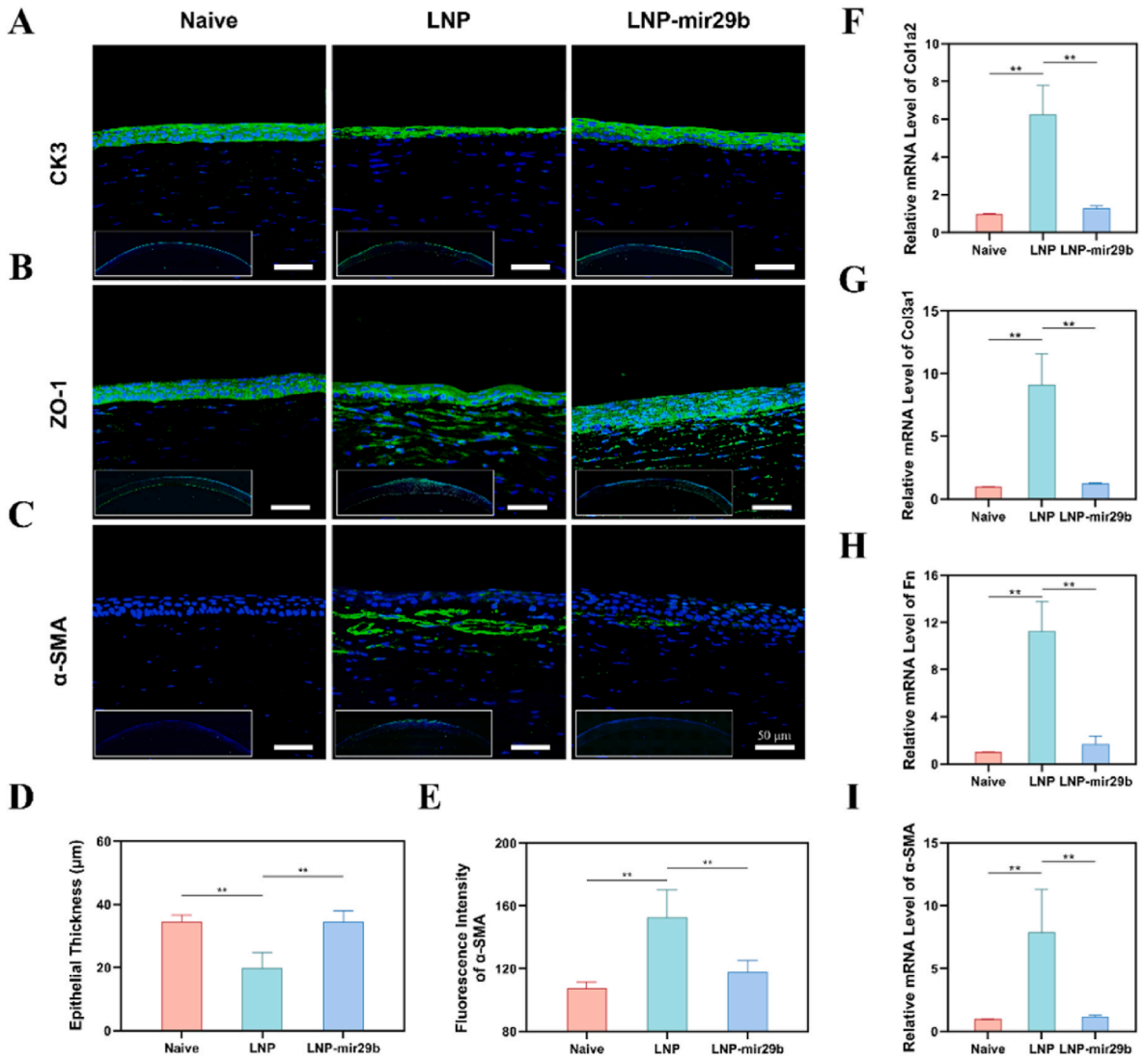

Fig. 6. LNP-mir29b promotes corneal epithelial structure recovery and reduces fibrotic proteins and genes expression post-operation in rabbits *in vivo*. Representative immunofluorescent images of A) CK3, B) ZO-1, C) α-SMA staining on day 14 post-operation of Naïve, LNP and LNP-mir29b groups. Scale bars: 50 μm. $n = 5$. D) Quantification of corneal thickness. $n = 5$, differences were compared to the naive group. E) Statistical analysis of α-SMA fluorescence intensity of Naïve, LNP, and LNP-mir29b groups. $n = 5$. The mRNA expression level of F), G) COL3A1, H) Fn, I) α-SMA on day 14 post-operation of Naïve, LNP, and LNP-mir29b groups. $n = 3$, $^{**}p < 0.01$.

in LNP group showed uneven thickness and unclear stratification, particularly in the central corneal region (Fig. 6D). Additionally, corneal epithelial cells in all groups expressed the Zonula Occludens-1 (ZO-1) protein. In the LNP-mir29b group, distinct tight junctions were formed on the epithelial surface, closely resembling those of the naive cornea (Fig. 6B). To quantify the level of fibrosis in the corneal stroma, α-SMA staining was conducted (Fig. 6C). The results demonstrated that α-SMA expression levels were significantly reduced in the LNP-mir29b group, showing no difference compared to the naive group. In contrast, the LNP group exhibited significantly elevated α-SMA expression levels (Fig. 6E). To further understand the mechanisms by which LNP-mir29b inhibited corneal scarring, the expression of corneal stromal scarring markers was investigated using quantitative PCR (qPCR) analysis. The results showed that the gene expression levels of Collagen Type I Alpha 2 Chain (Col1A2), Collagen Type III Alpha 1 Chain (Col3A1), Fibronectin (Fn), and α-SMA in the remodeled corneal tissues of LNP-mir29b group were significantly lower than those in LNP group and were not significantly different from those in naive group (Fig. 6F–I). Overall, the application of LNP-mir29b accelerated the recovery of the corneal epithelium, promoted the restoration of corneal epithelial structure, facilitated stromal regeneration, reduced the expression of fibrotic genes, and decreased scarring during the corneal injury repair process.

4. Discussion

Corneal scarring is a leading cause of corneal blindness, making the inhibition of scar formation during corneal wound healing a critical clinical need. Here, we present an LNP-based drug delivery system encapsulating miRNA29b, which effectively promotes the reduction of fibrosis during the repair of corneal epithelial-stromal mechanical injuries both *in vitro* and *in vivo* and accelerates epithelial healing and structural restoration. This promising approach could become a

significant ophthalmic topical treatment for achieving reduced scarring in corneal repair.

In this study, we employed LNP to encapsulate and deliver miRNA29b as a topical therapeutic for the cornea. Effective miRNA delivery systems must reach target cells and produce sufficient proteins, yet challenges such as targeted delivery and endosomal escape underscore the necessity of suitable delivery system. Notably, LNPs offer enhanced protection and stability for nucleic acid-based drugs [21]. Conventional methods for LNP production include microfluidics, thin-film hydration, sonication, and double emulsion techniques, each with distinct advantages and limitations [30]. Compared to other methods, microfluidic technology allows for the precise mixing of aqueous and organic lipid solutions, enabling controlled shear forces and fluid dynamics to produce uniformly sized LNP [31]. This method is well-suited for large-scale production, offering an advanced approach to LNP preparation that may be more suitable for future clinical applications, ultimately improving treatments for various corneal diseases [32].

Our study demonstrates that the LNP-mir29b system offers significant advantages for drug delivery in corneal injury repair. The ocular safety of LNPs has been substantiated in various studies, demonstrating their potential in treating a range of eye-related conditions, including posterior capsule opacification, age-related macular degeneration, and choroidal neovascularization [33,34]. Our *in vivo* results confirm that LNP-mir29b effectively localizes to the corneal wound site and infiltrates deeper corneal layers. LNP enhance drug stability and bioavailability while promoting effective corneal barrier penetration, further underscoring their potential in the development of novel ocular therapies [35].

To validate the anti-fibrotic effects of LNP-mir29b, we conducted both *in vitro* and *in vivo* experiments. Following corneal injury, corneal stromal cells undergo a phenotypic transformation into myofibroblasts, characterized by excessive α-SMA expression. This transformation leads to the synthesis and secretion of large amounts of collagen, resulting in a disordered collagen fiber arrangement and reduced corneal transparency [5]. Therefore, inhibiting α-SMA expression is crucial for preventing corneal fibrosis. The miRNA29 family has been found to reduce fibrosis in various tissues, including the heart [36], lungs [37], and liver [38,39], by downregulating fibrotic gene and protein expressions, particularly collagen and α-SMA [40]. However, its role in preventing corneal scarring remains to be fully elucidated. Studies have shown that exosomes from stem cells with high miRNA29 content exhibit superior antifibrotic effects *in vivo* [16,41]. Exosomes carrying miRNA29b-3p can activate autophagy, suppressing corneal inflammation and fibrosis [41]. However, their therapeutic efficacy may be influenced by other bioactive components within the exosomal contents. In contrast, our study employed LNP as a direct and controlled miRNA29b delivery system, allowing for a targeted evaluation of its antifibrotic effects in corneal injury. Furthermore, we confirmed that its antifibrotic effect in corneal tissue is achieved through the downregulation of collagen and α-SMA expression.

Remarkably, our study revealed that LNP-mir29b plays a dual role in anti-corneal stromal fibrosis and facilitating epithelial wound healing. Cell migration is a critical factor in epithelial wound healing, as it allows rapid re-epithelialization and structural recovery. Previous studies have reported that miRNA29 plays a role in tissue repair; however, its effects on corneal epithelial cell migration have not been extensively investigated. To the best of our knowledge, this is the first study to suggest a potential role for miRNA29 in corneal epithelial migration and repair. Researches on miRNA29 have shown that the effect on cell migration vary across different cell types. For instance, miRNA29 promotes migration in osteosarcoma cells but inhibits in airway epithelial cells and various cancer cells, which necessitates analysis in the context of specific tissue functions [42–45]. Its role in corneal epithelial migration may be influenced by tissue-specific signaling pathways. Upon injury, corneal epithelial cells release various cytokines and growth factors, such as TGF-β1, which induce stromal cells to transform into myofibroblasts via autocrine and paracrine mechanisms [46,47]. Rapid epithelial repair is thus vital for stromal reconstruction and the restoration of corneal transparency. Additionally, the healthy corneal epithelium consists of three distinct layers: basal cells, wing cells, and superficial cells [48]. Each of these cell layers serves specific functions, working together to ensure corneal integrity and function by replacing damaged cells and protecting the cornea from environmental harm. The re-establishment of a structurally intact epithelial layer is therefore essential for maintaining corneal homeostasis and visual clarity. Currently, the mechanisms by which miRNA29 influences cell migration have been reported to vary across different tissues. It may regulate cell migration through various pathways, including the modulation of the p53/ADAM12 axis [49], the PTEN/PI3K pathway [50], and targeting the VSIG1/ZO-1 axis [51], among others. Therefore, elucidating the specific mechanisms by which miRNA29 affects corneal epithelial cell migration could be an important direction for future research. *In vivo*, corneal epithelial wound healing is closely related to the properties of the corneal stroma. Disorganized collagen fiber organization and abnormal extracellular matrix stiffness can reduce the speed and efficiency of corneal epithelial cell migration [52,53], induce epithelial cell apoptosis [54], and impair cell adhesion [55,56], ultimately leading to delayed epithelial repair. Our results indicate that miRNA29 promotes the restoration of corneal thickness and structural integrity, which may contribute to enhanced corneal epithelial wound healing. However, the *in vivo* corneal environment is highly complex, and the precise mechanisms underlying these processes require further investigation.

This study is the first to propose the use of LNP-mir29b for repairing corneal mechanical injuries. LNP-mir29b has demonstrated good biocompatibility and therapeutic efficacy in both *in vitro* and *in vivo* experiments. LNP-mir29b inhibited the transformation of corneal stromal cells into fibroblasts, reducing the expression of genes and proteins associated with corneal scarring, thereby promoting scarless repair after corneal injury. Additionally, LNP-mir29b promotes the migration of corneal epithelial cells, accelerating the healing of epithelial wounds and facilitating the restoration of the structural integrity of the corneal epithelium. However, this study has several limitations. The molecular mechanisms underlying LNP-mir29b's anti-fibrotic effects and its role in promoting corneal epithelial healing have not been thoroughly investigated and warrant further study. Additionally, future research could focus on labeling LNP-mir29b to obtain clearer evidence of its penetration and localized concentration within the corneal tissue.

5. Conclusion

We developed an LNP-based delivery system for miRNA29b and demonstrated its effective antifibrotic properties and its ability to promote corneal injury repair both *in vivo* and *in vitro*. Additionally, we were the first to discover the promotive effects of miRNA29b on corneal epithelial cell migration and epithelial tissue repair. In conclusion, LNP-mir29b prevented extracellular matrix deposition, reduced corneal fibrosis during the corneal injury repair process, and maintained high transparency of the treated corneal tissue. As an effective topical therapeutic agent, LNP-mir29b holds significant promise for combating corneal scarring and promoting corneal injury repair, with substantial potential for clinical application in ophthalmology.

List of Abbreviation

Abbreviation	Full Term
α-SMA	α-smooth muscle actin
AS-OCT	Anterior segment optical coherence tomography
CCK-8	Cell counting kit-8
CK3	Cytokeratin 3
COL1A2	Collagen type I Alpha 2 chain
COL3A1	Collagen type III Alpha 1 chain
DLin-MC3-DMA	1,2-dilinoleyloxy-3-dimethylaminopropane
DMEM/F12	Dulbecco's Modified Eagle Medium/Nutrient mixture F-12 medium
DMG-PEG2000	1,2-dimyristoyl-rac-glycero-3-methoxypolyethylene glycol-2000
DSPC	1,2-distearoyl-sn-glycero-3-phosphocholine
EVG	Elastica van gieson
FBS	Fetal bovine serum
Fn	Fibronectin
HCE-T	Human corneal epithelial cells
HE	Hematoxylin and eosin
hEGF	Human epidermal growth factor
LNP-mir29b	LNP-miRNA29b delivery system
LNPs	Lipid nanoparticles
miRNA	MicroRNA
PAS	Periodic acid-schiff
PBS	Phosphate-buffered saline
RCSC	Primary rabbit corneal stromal cells
RCSF	Primary rabbit corneal stromal fibroblasts
TEM	Transmission electron microscope
TGF-β1	Transforming growth factor β1
ZO-1	Zonula occludens-1

CRediT authorship contribution statement

Dongyan Li: Writing – original draft, Conceptualization. **Jing Ji:** Writing – review & editing, Conceptualization. **Xinyue Li:** Methodology. **Yi Xie:** Data curation. **Yan Huang:** Methodology. **Junzhi Qin:** Formal analysis. **Xili Ding:** Writing – review & editing, Conceptualization. **Lizhen Wang:** Data curation. **Yubo Fan:** Writing – review & editing, Conceptualization.

Statement of significance

Severe corneal injuries result in scarring, leading to visual impairment and even blindness. Current therapeutic strategies for corneal scarring remain inadequate. We proposed a novel approach using lipid nanoparticles (LNP) to encapsulate and deliver microRNA29b as an LNP-mir29b delivery system (LNP-mir29b), applying microRNA29b as an independent therapeutic agent for the first time in the treatment of corneal would healing. LNP-mir29b was efficiently delivered to the injury site, significantly reducing scar formation and improving corneal transparency during the repair process. Moreover, we were the first to discover that microRNA29b exhibited promotive effects on corneal epithelial cell migration and epithelial tissue repair. This study provides an approach using microRNA29b for localized treatment, capable of inhibiting corneal scarring and restoring comprehensive corneal integrity.

Funding

This work was supported by National Key Research and Development Program of China [grant numbers 2023YFC2410404], Beijing Municipal Natural Science Foundation [grant numbers. Z240017], National Natural Science Foundation of China [grant numbers 12472316, 12232019, 12332019, 12372311], Fundamental Research Funds for the Central Universities.

Declaration of competing interest

The authors declare that they have no known competing financial interests or personal relationships that could have appeared to influence the work reported in this paper.

Appendix A. Supplementary data

Supplementary data to this article can be found online at https://doi.org/10.1016/j.mtbio.2025.101695.

Data availability

Data will be made available on request.

References

[1] M.J. Burton, J. Ramke, A.P. Marques, R.R.A. Bourne, N. Congdon, I. Jones, B.A. M. Ah Tong, S. Arunga, D. Bachani, C. Bascaran, A. Bastawrous, K. Blanchet, T. Braithwaite, J.C. Buchan, J. Cairns, A. Cama, M. Chagunda, C. Chuluunkhuu, A. Cooper, J. Crofts-Lawrence, W.H. Dean, A.K. Denniston, J.R. Ehrlich, P. M. Emerson, J.R. Evans, K.D. Frick, D.S. Friedman, J.M. Furtado, M.M. Gichangi, S. Gichuhi, S.S. Gilbert, R. Gurung, E. Habtamu, P. Holland, J.B. Jonas, P.A. Keane, L. Keay, R.C. Khanna, P.T. Khaw, H. Kuper, F. Kyari, V.C. Lansingh, I. Mactaggart, M.M. Mafwiri, W. Mathenge, I. McCormick, P. Morjaria, L. Mowatt, D. Muirhead, G.V.S. Murthy, N. Mwangi, D.B. Patel, T. Peto, B.M. Qureshi, S.R. Salomão, V. Sarah, B.R. Shilio, A.W. Solomon, B.K. Swenor, H.R. Taylor, N. Wang, A. Webson, S.K. West, T.Y. Wong, R. Wormald, S. Yasmin, M. Yusufu, J.C. Silva, S. Resnikoff, T. Ravilla, C.E. Gilbert, A. Foster, H.B. Faal, The lancet global health commission on global eye health: vision beyond 2020, Lancet Global Health 9 (2021) e489–e551, https://doi.org/10.1016/S2214-109X(20)30488-5.

[2] B. Barrientez, S.E. Nicholas, A. Whelchel, R. Sharif, J. Hjortdal, D. Karamichos, Corneal injury: clinical and molecular aspects, Exp. Eye Res. 186 (2019) 107709, https://doi.org/10.1016/j.exer.2019.107709.

[3] S. Matthyssen, B. Van den Bogerd, S.N. Dhubhghaill, C. Koppen, N. Zakaria, Corneal regeneration: a review of stromal replacements, Acta Biomater. 69 (2018) 31–41, https://doi.org/10.1016/j.actbio.2018.01.023.

[4] K.M. Meek, C. Knupp, Corneal structure and transparency, Prog. Retin. Eye Res. 49 (2015) 1–16, https://doi.org/10.1016/j.preteyeres.2015.07.001.

[5] S.E. Wilson, L.P. Sampaio, T.M. Shiju, G.S.L. Hilgert, R.C. de Oliveira, Corneal opacity: cell biological determinants of the transition from transparency to transient haze to scarring fibrosis, and resolution, after injury, Investig. Ophthalmol. Vis. Sci. 63 (2022) 22, https://doi.org/10.1167/iovs.63.1.22.

[6] R.R. Mohan, D. Kempuraj, S. D'Souza, A. Ghosh, Corneal stromal repair and regeneration, Prog. Retin. Eye Res. 91 (2022) 101090, https://doi.org/10.1016/j.preteyeres.2022.101090.

[7] E. Arranz-Marquez, A. Katsanos, V.P. Kozobolis, A.G.P. Konstas, M.A. Teus, A critical overview of the biological effects of mitomycin C application on the cornea following refractive surgery, Adv. Ther. 36 (2019) 786–797, https://doi.org/10.1007/s12325-019-00905-w.

[8] P. Gain, R. Jullienne, Z. He, M. Aldossary, S. Acquart, F. Cognasse, G. Thuret, Global survey of corneal transplantation and eye banking, JAMA Ophthalmol 134 (2016) 167–173, https://doi.org/10.1001/jamaophthalmol.2015.4776.

[9] P.T.B. Ho, I.M. Clark, L.T.T. Le, MicroRNA-based diagnosis and therapy, Int. J. Mol. Sci. 23 (2022) 7167, https://doi.org/10.3390/ijms23137167.

[10] P.M. Robinson, T.-D. Chuang, S. Sriram, L. Pi, X.P. Luo, B.E. Petersen, G.S. Schultz, MicroRNA signature in wound healing following excimer laser ablation: role of miR-133b on TGFβ1, CTGF, SMA, and COL1A1 expression levels in rabbit corneal fibroblasts, Investig. Ophthalmol. Vis. Sci. 54 (2013) 6944–6951, https://doi.org/10.1167/iovs.13-12621.

[11] Z. Deng, Y. He, X. Yang, H. Shi, A. Shi, L. Lu, L. He, MicroRNA-29: a crucial player in fibrotic disease, Mol. Diagn. Ther. 21 (2017) 285–294, https://doi.org/10.1007/s40291-016-0253-9.

[12] C. Li, N. Wang, P. Rao, L. Wang, D. Lu, L. Sun, Role of the MicroRNA-29 family in myocardial fibrosis, J. Physiol. Biochem. 77 (2021) 365–376, https://doi.org/10.1007/s13105-021-00814-z.

[13] Y. Matsumoto, S. Itami, M. Kuroda, K. Yoshizato, N. Kawada, Y. Murakami, MiR-29a assists in preventing the activation of human stellate cells and promotes recovery from liver fibrosis in mice, Mol. Ther. 24 (2016) 1848–1859, https://doi.org/10.1038/mt.2016.127.

[14] M. Chioccioli, S. Roy, R. Newell, L. Pestano, B. Dickinson, K. Rigby, J. Herazo-Maya, G. Jenkins, S. Ian, G. Saini, S.R. Johnson, R. Braybrooke, G. Yu, M. Sauler, F. Ahangari, S. Ding, J. DeIuliis, N. Aurelien, R.L. Montgomery, N. Kaminski, A lung targeted MiR-29 mimic as a therapy for pulmonary fibrosis, EBioMedicine 85 (2022) 104304, https://doi.org/10.1016/j.ebiom.2022.104304.

[15] C.L. Gallant-Behm, J. Piper, J.M. Lynch, A.G. Seto, S.J. Hong, T.A. Mustoe, C. Maari, L.A. Pestano, C.M. Dalby, A.L. Jackson, P. Rubin, W.S. Marshall, A MicroRNA-29 mimic (remlarsen) represses extracellular matrix expression and fibroplasia in the skin, J. Invest. Dermatol. 139 (2019) 1073–1081, https://doi.org/10.1016/j.jid.2018.11.007.

[16] G.H.-F. Yam, T. Yang, M.L. Geary, M. Santra, M. Funderburgh, E. Rubin, Y. Du, J. A. Sahel, V. Jhanji, J.L. Funderburgh, Human corneal stromal stem cells express anti-fibrotic MicroRNA-29a and 381-5p – a robust cell selection tool for stem cell therapy of corneal scarring, J. Adv. Res. 45 (2023) 141–155, https://doi.org/10.1016/j.jare.2022.05.008.
[17] M. Scheideler, I. Vidakovic, R. Prassl, Lipid nanocarriers for MicroRNA delivery, Chem. Phys. Lipids 226 (2020) 104837, https://doi.org/10.1016/j.chemphyslip.2019.104837.
[18] M. Mobaraki, M. Soltani, S. Zare Harofte, E.L. Zoudani, R. Daliri, M. Aghamirsalim, K. Raahemifar, Biodegradable nanoparticle for cornea drug delivery: focus review, Pharmaceutics 12 (2020) 1232, https://doi.org/10.3390/pharmaceutics12121232.
[19] R. Suri, S. Beg, K. Kohli, Target strategies for drug delivery bypassing ocular barriers, J. Drug Deliv. Sci. Technol. 55 (2020) 101389, https://doi.org/10.1016/j.jddst.2019.101389.
[20] P.R. Cullis, M.J. Hope, Lipid nanoparticle systems for enabling gene therapies, Mol. Ther. 25 (2017) 1467–1475, https://doi.org/10.1016/j.ymthe.2017.03.013.
[21] X. Hou, T. Zaks, R. Langer, Y. Dong, Lipid nanoparticles for mRNA delivery, Nat. Rev. Mater. 6 (2021) 1078–1094, https://doi.org/10.1038/s41578-021-00358-0.
[22] J.C. Kaczmarek, P.S. Kowalski, D.G. Anderson, Advances in the delivery of RNA therapeutics: from concept to clinical reality, Genome Med. 9 (2017) 60, https://doi.org/10.1186/s13073-017-0450-0.
[23] Y. Zong, Y. Lin, T. Wei, Q. Cheng, Lipid nanoparticle (LNP) enables mRNA delivery for cancer therapy, Adv. Mater. 35 (2023) e2303261, https://doi.org/10.1002/adma.202303261.
[24] S. Patel, R.C. Ryals, K.K. Weller, M.E. Pennesi, G. Sahay, Lipid nanoparticles for delivery of messenger RNA to the back of the eye, J. Contr. Release 303 (2019) 91–100, https://doi.org/10.1016/j.jconrel.2019.04.015.
[25] H. Zhang, J. Leal, M.R. Soto, H.D.C. Smyth, D. Ghosh, Aerosolizable lipid nanoparticles for pulmonary delivery of mRNA through design of experiments, Pharmaceutics 12 (2020) 1042, https://doi.org/10.3390/pharmaceutics12111042.
[26] K. Gokita, J. Inoue, H. Ishihara, K. Kojima, J. Inazawa, Therapeutic potential of LNP-mediated delivery of miR-634 for cancer therapy, Mol. Ther. Nucleic Acids 19 (2020) 330–338, https://doi.org/10.1016/j.omtn.2019.10.045.
[27] F. Wang, W. Zhang, Y. Qiao, D. Shi, L. Hu, J. Cheng, J. Wu, L. Zhao, D. Li, W. Shi, L. Xie, Q. Zhou, ECM-like adhesive hydrogel for the regeneration of large corneal stromal defects, Adv. Healthcare Mater. 12 (2023) 2300192, https://doi.org/10.1002/adhm.202300192.
[28] C. Cejka, T. Ardan, J. Sirc, J. Michálek, B. Brůnová, J. Cejková, The influence of various toxic effects on the cornea and changes in corneal light transmission, Graefes Arch. Clin. Exp. Ophthalmol. 248 (2010) 1749–1756, https://doi.org/10.1007/s00417-010-1438-2.
[29] C. Peris-Martínez, M.C. García-Domene, M. Penadés, M.J. Luque, E. Fernández-López, J.M. Artigas, Spectral transmission of the human corneal layers, J. Clin. Med. 10 (2021) 4490, https://doi.org/10.3390/jcm10194490.
[30] M. Mehta, T.A. Bui, X. Yang, Y. Aksoy, E.M. Goldys, W. Deng, Lipid-based nanoparticles for drug/gene delivery: an overview of the production techniques and difficulties encountered in their industrial development, ACS Mater. Au 3 (2023) 600–619, https://doi.org/10.1021/acsmaterialsau.3c00032.
[31] A. Vogelaar, S. Marcotte, J. Cheng, B. Oluoch, J. Zaro, Use of microfluidics to prepare lipid-based nanocarriers, Pharmaceutics 15 (2023) 1053, https://doi.org/10.3390/pharmaceutics15041053.
[32] D. S, A. N, V. Tf, S. Ca, Microfluidic nanoprecipitation systems for preparing pure drug or polymeric drug loaded nanoparticles: an overview, Expet Opin. Drug Deliv. 13 (2016), https://doi.org/10.1080/17425247.2016.1193151.
[33] T. Wang, T. Yu, Q. Liu, T.-C. Sung, A. Higuchi, Lipid nanoparticle technology-mediated therapeutic gene manipulation in the eyes, Mol. Ther. Nucleic Acids 35 (2024), https://doi.org/10.1016/j.omtn.2024.102236.
[34] S. Zeng, Y. Chen, F. Zhou, T. Zhang, X. Fan, W. Chrzanowski, M.C. Gillies, L. Zhu, Recent advances and prospects for lipid-based nanoparticles as drug carriers in the treatment of human retinal diseases, Adv. Drug Deliv. Rev. 199 (2023) 114965, https://doi.org/10.1016/j.addr.2023.114965.
[35] C. Chapa González, J.V. Martínez Saráoz, J.A. Roacho Pérez, I. Olivas Armendáriz, Lipid nanoparticles for gene therapy in ocular diseases, Daru 31 (2023) 75–82, https://doi.org/10.1007/s40199-023-00455-1.
[36] J. Yuan, H. Yang, C. Liu, L. Shao, H. Zhang, K. Lu, J. Wang, Y. Wang, Q. Yu, Y. Zhang, Y. Yu, Z. Shen, Microneedle patch loaded with exosomes containing MicroRNA-29b prevents cardiac fibrosis after myocardial infarction, Adv. Healthcare Mater. 12 (2023) e2202959, https://doi.org/10.1002/adhm.202202959.
[37] P. Li, X. Hao, J. Liu, Q. Zhang, Z. Liang, X. Li, H. Liu, MiR-29a-3p regulates autophagy by targeting Akt3-mediated mTOR in SiO2-induced lung fibrosis, Int. J. Mol. Sci. 24 (2023) 11440, https://doi.org/10.3390/ijms241411440.
[38] B.J. Asl, S. Monjezi, G. Orak, F. Ghaffari, S.S. Bavarsad, N. Dinarvand, A. Khedri, The up-regulation of miR-146a and miR-29b via exosomes protects against liver fibrosis by inhibiting the TGF-β/Smad3c signaling pathway, Hepat. Mon. 24 (2024), https://doi.org/10.5812/hepatmon-144095.
[39] K. Matsumoto, Y. Ohsugi, C. Tayama, M. Hayashi, Y. Kato, M. Ohashi, M. Chiba, Serum MiR-29 is increased in mice with early liver fibrosis, Exp. Ther. Med. 28 (2024) 285, https://doi.org/10.3892/etm.2024.12573.
[40] Y. He, C. Huang, X. Lin, J. Li, MicroRNA-29 family, A crucial therapeutic target for fibrosis diseases, Biochimie 95 (2013) 1355–1359, https://doi.org/10.1016/j.biochi.2013.03.010.
[41] J. Liu, J. Gao, P. Lu, Y. Wang, S. Xing, Y. Yan, R. Han, P. Hao, X. Li, Mesenchymal stem cell-derived exosomes as drug carriers for delivering miRNA-29b to ameliorate inflammation in corneal injury via activating autophagy, Investig. Ophthalmol. Vis. Sci. 65 (2024) 16, https://doi.org/10.1167/iovs.65.6.16.
[42] Q. Liu, P. Geng, L. Shi, Q. Wang, P. Wang, MiR-29 promotes osteosarcoma cell proliferation and migration by targeting PTEN, Oncol. Lett. 17 (2019) 883–890, https://doi.org/10.3892/ol.2018.9646.
[43] T. Kinoshita, N. Nohata, T. Hanazawa, N. Kikkawa, N. Yamamoto, H. Yoshino, T. Itesako, H. Enokida, M. Nakagawa, Y. Okamoto, N. Seki, Tumour-suppressive MicroRNA-29s inhibit cancer cell migration and invasion by targeting laminin-integrin signalling in head and neck squamous cell carcinoma, Br. J. Cancer 109 (2013) 2636–2645, https://doi.org/10.1038/bjc.2013.607.
[44] H. Wang, Y. Zhu, M. Zhao, C. Wu, P. Zhang, L. Tang, H. Zhang, X. Chen, Y. Yang, G. Liu, MiRNA-29c suppresses lung cancer cell adhesion to extracellular matrix and metastasis by targeting integrin β1 and matrix Metalloproteinase2 (MMP2), PLoS One 8 (2013) e70192, https://doi.org/10.1371/journal.pone.0070192.
[45] J.-M. Shin, J.-H. Park, H.-W. Yang, J.W. Moon, H.-M. Lee, I.-H. Park, MiR-29b regulates TGF-β1-induced epithelial-mesenchymal transition by inhibiting heat shock protein 47 expression in airway epithelial cells, Int. J. Mol. Sci. 22 (2021) 11535, https://doi.org/10.3390/ijms222111535.
[46] K.E. Tarvestad-Laise, B.P. Ceresa, Modulating growth factor receptor signaling to promote corneal epithelial homeostasis, Cells 12 (2023) 2730, https://doi.org/10.3390/cells12232730.
[47] S.E. Wilson, Corneal wound healing, Exp. Eye Res. 197 (2020) 108089, https://doi.org/10.1016/j.exer.2020.108089.
[48] P. Bhattacharya, K. Edwards, K.L. Schmid, Regional variations in corneal epithelial cell density and morphology assessed using in vivo confocal microscopy, Eye Contact Lens 50 (2024) 163, https://doi.org/10.1097/ICL.0000000000001067.
[49] J. Che, Z. Su, W. Yang, L. Xu, Y. Li, H. Wang, W. Zhou, Tumor-suppressor p53 specifically binds to MiR-29c-3p and reduces ADAM12 expression in hepatocellular carcinoma, Dig. Liver Dis. 55 (2023) 412–421, https://doi.org/10.1016/j.dld.2022.05.014.
[50] W. Zhang, Q. Wu, Y. Liu, X. Wang, C. Ma, W. Zhu, LncRNA HOTAIR promotes chemoresistance by facilitating epithelial to mesenchymal transition through miR-29b/PTEN/PI3K signaling in cervical cancer, Cells Tissues Organs 211 (2022) 16–29, https://doi.org/10.1159/000519844.
[51] C. Wu, D. Li, X. Cheng, H. Gu, Y. Qian, L. Feng, Downregulation of cancer-associated fibroblast exosome-derived MiR-29b-1-5p restrains vasculogenic mimicry and apoptosis while accelerating migration and invasion of gastric cancer cells via immunoglobulin domain-containing 1/zonula occluden-1 Axis, Cell Cycle 22 (2023) 1807–1826, https://doi.org/10.1080/15384101.2023.2231740.
[52] K.A. Diehl, J.D. Foley, P.F. Nealey, C.J. Murphy, Nanoscale topography modulates corneal epithelial cell migration, J. Biomed. Mater. Res. A 75A (2005) 603–611, https://doi.org/10.1002/jbm.a.30467.
[53] K. Jaskiewicz, M. Maleszka-Kurpiel, E. Matuszewska, M. Kabza, M. Rydzanicz, R. Malinowski, R. Ploski, J. Matysiak, M. Gajecka, The impaired wound healing process is A major factor in remodeling of the corneal epithelium in adult and adolescent patients with keratoconus, invest, Ophthalmol. Vis. Sci. 64 (2023) 22, https://doi.org/10.1167/iovs.64.2.22, 22.
[54] S. Kling, F. Hafezi, Corneal biomechanics – a review, Ophthalmic Physiol. Opt. 37 (2017) 240–252, https://doi.org/10.1111/opo.12345.
[55] S. Molladavoodi, H.-J. Kwon, J. Medley, M. Gorbet, Human corneal epithelial cell response to substrate stiffness, Acta Biomater. 11 (2015) 324–332, https://doi.org/10.1016/j.actbio.2014.10.005.
[56] O.E. Onochie, A. Zollinger, C.B. Rich, M. Smith, V. Trinkaus-Randall, Epithelial cells exert differential traction stress in response to substrate stiffness, Exp. Eye Res. 181 (2019) 25–37, https://doi.org/10.1016/j.exer.2019.01.014.